Design of a High-Voltage High-Frequency Insulation Test System Using a Ferrite-Based Oil-Insulated Resonant Transformer

Zhao, Weichuan; Lagerweij, Gijs Willem; Niasar, Mohamad Ghaffarian

DOI
10.1049/hve2.70038

Publication date
2025

Document Version
Final published version

Published in
High Voltage

Citation (APA)
Zhao, W., Lagerweij, G. W., & Niasar, M. G. (2025). Design of a High-Voltage High-Frequency Insulation Test System Using a Ferrite-Based Oil-Insulated Resonant Transformer. *High Voltage*, *10*(5), 1247-1256. https://doi.org/10.1049/hve2.70038

High Voltage

WILEY

国家电网 STATE GRID 中国电力科学研究院有限公司 CHINA ELECTRIC POWER RESEARCH INSTITUTE | IET The Institution of Engineering and Technology

ORIGINAL RESEARCH OPEN ACCESS

Design of a High-Voltage High-Frequency Insulation Test System Using a Ferrite-Based Oil-Insulated Resonant Transformer

Weichuan Zhao[1] | Gijs Willem Lagerweij[2] | Mohamad Ghaffarian Niasar[1]

[1]High Voltage Technologies, Electrical Sustainable Energy, Delft University of Technology, Delft, the Netherlands | [2]Prodrive Technologies, Son, the Netherlands

Correspondence: Mohamad Ghaffarian Niasar (m.ghaffarianniasar@tudelft.nl)

Received: 18 June 2024 | **Revised:** 22 August 2024 | **Accepted:** 25 September 2024

Associate Editor: Jun Jiang

Funding: This study was supported by TKI Urban Energy (Grant 1821403).

ABSTRACT

As power-electronic (PE)-based systems become increasingly common in the electric power grid, the insulation systems used in medium- and high-voltage (HV) applications will be exposed to high-frequency (HF) electric fields. Therefore, the insulation materials must be characterised using HF waveforms. However, generating these waveforms presents a significant challenge due to the large reactive power associated with the dv/dt. This paper proposes a resonant test system with a ferrite-based transformer for HF insulation testing. The resonant circuit is formed by the transformer's leakage inductance and the insulation sample capacitance, with an adjustable frequency tuning capacitor. The system can be driven with an inverter or linear power amplifier. Increasing the test voltage level while maintaining the same test frequency presents several challenges: transformer core grounding, high resonant current and implications for bobbin and insulation design. This paper investigates these challenges and proposes an oil-insulated resonant transformer, capable of extending the test voltage to 23 kV_{pk} for HF insulation tests at around 40 kHz. High-frequency breakdown tests are performed on enamelled copper wire in various insulation media using the prototype resonant test system, highlighting the importance of the dielectric's thermal performance.

1 | Introduction

With the increasing introduction of PE-based systems in the electricity grid, both medium- and high-voltage (HV) insulation systems are subjected to voltage waveforms containing high-frequency (HF) components in the kHz and MHz range. This HF content results in an accelerated insulation degradation, potentially reducing the lifetime by orders of magnitude. Therefore, insulation materials must be characterised and tested using HF waveforms. The major challenge in generating the HV-HF waveforms is the enormous reactive power associated with the dv/dt, even for capacitances in the range of hundreds of pF [1].

Although the insulation systems for PE-based components typically experience pulsed stress, they can be characterised with HV-HF sinusoidal waveforms, which are easier to generate at the required frequencies. The following methods have been used to generate such waveforms:

- Linear HV amplifier: Linear amplifiers are limited in the available output current (HV side) and, thus, cannot be used beyond several kHz. For example, with an HV power amplifier of type Trek Model 30-20A, voltage levels up to about 25 kV_{pk} can be attained at frequencies less than 2.5 kHz with acceptable distortion [2].

- PE-based HV source: HV arbitrary waveform generators for insulation testing are currently under development. The bandwidth and the output voltage level are still limited by the available hardware [3–5].
- Vacuum tube oscillator: An oscillator with HV output can be built with a high-power vacuum tube and resonant anode circuit. Frequencies up to 5 MHz may be achieved, but the voltage is limited by the tube and losses in the resonant circuit [6, 7].
- Inverter- or amplifier-driven transformer: Linear power amplifiers and inverters are easy to obtain. In combination with a simple resonant transformer, the authors could generate high voltages (approx. 10 kV_{pk}) at frequencies in the range of 10–100 kHz [1, 8].

For decades, HV test systems for power-frequency AC have utilised (quasi-)resonant circuits to compensate (a part of) the current drawn by large capacitive loads presented by, for example, cables and transformers [9, 10]. This concept can be applied to achieve full resonance at any desired testing frequency [11, 12]. In this paper, a resonant system is developed which can be driven by an inverter or power amplifier for HV testing at high frequencies ranging from 30 to 45 kHz.

1.1 | State-of-the-Art

An air-coupled (or Tesla) transformer has sometimes been used for HV-HF testing [12]. These transformers are rather big and less easily controlled than, for example, a transformer using a ferrite core. Ferrite-based resonant transformers are small, easy to build and drive and cheap [8]. However, ferrite-based resonance transformers are usually not chosen due to (i) the nonlinearity of the core material at high flux density and (ii) the parasitic capacitance of the transformer, which can restrict the tunable frequency range compared to a Tesla transformer-based solution. This paper will further explore the advantages and disadvantages in HF insulation testing.

The general architecture of the described resonant test system is shown in Figure 1. The key component is a ferrite-core transformer whose secondary leakage inductance L_σ creates a resonant circuit with the insulation sample (DUT), modelled as the capacitance C_{DUT}. The resonance frequency can be tuned using an additional adjustable capacitor C_{res}. The losses in the resonant transformer and DUT have a significant effect on the gain of this system. Due to its resonant nature, the test system can be driven with any waveform as long as it has a frequency component at the resonant frequency. Therefore, it is possible to drive the system with a switching (PE-based) pulse generator or a (linear) power amplifier.

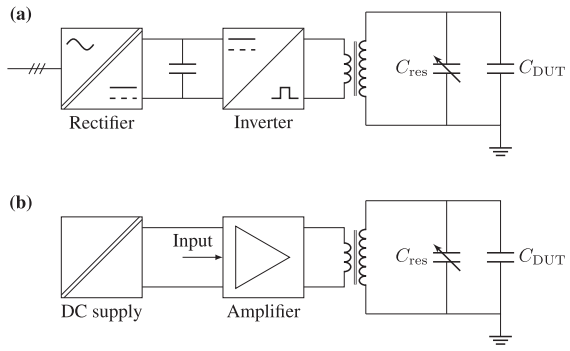

FIGURE 1 | Insulation test system with an HV resonant transformer utilising (a) PE-based pulse generator, (b) power amplifier.

Most available literature on HF ageing of insulating materials is limited to high frequency and medium voltage (several kV) or medium frequency and high voltage (several tens of kV). A series-resonant test system is proposed to extend the testable range. The design of such resonant test systems up to a voltage of 10 kV_{pk} and several tens to 100 kHz can be achieved using extremely simple means, as demonstrated in refs. [1, 8]. This paper shows that several big challenges must be overcome to increase the output voltage to around 23 kV_{pk} while maintaining the same test frequency.

1.2 | Outline

In Section 2, two analytical models are derived for the test system to explain the effect of the various circuit parameters on the gain of the system. The resonant transformer design is discussed in Section 3 using a model-based approach. When increasing the frequency, the current drawn by the DUT will naturally increase. Even for very small DUTs, the reactive power may exceed the single-digit kVAs. The combination of high current and high voltage in the limited window area results in a complex secondary winding design. Section 4 addresses the implications for the bobbin and insulation design. A transformer prototype is built and evaluated in Section 5. The prototype is then used to perform breakdown tests, which show the importance of the dielectric loss and cooling performance of the insulation. Finally, Sections 6 and 7 provide a discussion on the encountered issues and a conclusion on the suitability of the designed system for insulation testing using HF sinusoidal voltage.

2 | Resonant Test System Circuit Analysis

2.1 | Resonant Transformer With Ideal DUT

Ideally, the DUT can be modelled as a lossless capacitor C_{DUT}. Substituting the well-known equivalent circuit for the transformer (leakage inductances L_{11} and L_{22}, magnetising inductance L_m and winding resistances R_{11} and R_{21}) and referring all the components to the secondary side yield the circuit in Figure 2. The input voltage u_i in the Laplace domain (with variable s) is transformed to the secondary side by multiplication with n. The output u_o is taken across C_{eq}.

These components can be lumped together into an effective transfer ratio m and a damped series RLC circuit composed of L_{eq}, C_{eq} and R_{eq}.

$$m = \frac{nL''_m}{L''_m + L''_{11}}, \tag{1}$$

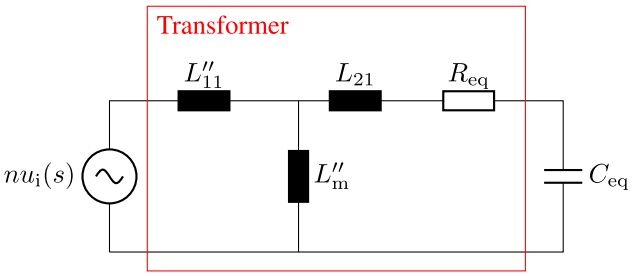

FIGURE 2 | Equivalent circuit of the resonant transformer-based test system. L''_m and L''_{11} are referred to the secondary side.

$$L_{eq} = L_{21} + L''_m \| L''_{11}, \tag{2}$$

$$R_{eq} = R_{21} + R''_{11}, \tag{3}$$

$$C_{eq} = C_{DUT} + C_{res} + C_\sigma, \tag{4}$$

In a transformer with a magnetic core, usually $L_m \gg L_{11}$. Therefore, the resonant system can be modelled using the second-order transfer function (5) in terms of the natural frequency ω_0 and damping factor ζ.

$$\frac{u_o(s)}{u_i(s)} = \frac{m\omega_0^2}{s^2 + 2\zeta\omega_0 + \omega_0^2}, \tag{5}$$

$$\omega_0 = \frac{1}{\sqrt{L_{eq}C_{eq}}}, \tag{6}$$

$$\zeta = \frac{R_{eq}}{2\omega_0 L_{eq}} = \frac{R_{eq}}{2}\sqrt{\frac{C_{eq}}{L_{eq}}}. \tag{7}$$

2.2 | Resonant Transformer With Lossy DUT

In practice, the DUT is not perfectly capacitive, and an additional loss component must be considered. The origin of this loss can be the dielectric loss (tan δ), partial discharges or conductivity of the dielectric. The loss is modelled with an additional resistance R_p in parallel with the DUT capacitance. The transfer function of the equivalent circuit in Figure 3 is given in Equation (8). By reducing R_p (i.e., increasing loss), the damping of the circuit is increased, and the resonance frequency drops.

$$\frac{u_o(s)}{u_i(s)} = \frac{m\omega_0^2}{s^2 + s\left(\frac{R_{eq}}{L_{eq}} + \frac{1}{R_p C_{eq}}\right) + \omega_0^2\left(\frac{R_{eq}}{R_p} + 1\right)}. \tag{8}$$

In the most general case, R_p will be a function of frequency, voltage, temperature and other environmental influences. To accurately predict the output voltage of the test system, dielectric loss and partial discharges should be accounted for.

3 | Transformer Design Procedure

The capabilities of the resonant test system are limited in part by the transformer design. They may be evaluated in terms of the load diagram (Figure 4), which is also typically provided for low-frequency resonant test systems [10]. The transformer design aspects influencing this diagram are

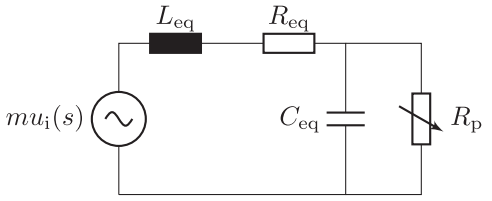

FIGURE 3 | Equivalent circuit of the resonant transformer-based test system. The lossy DUT is modelled as a parallel *RC* circuit.

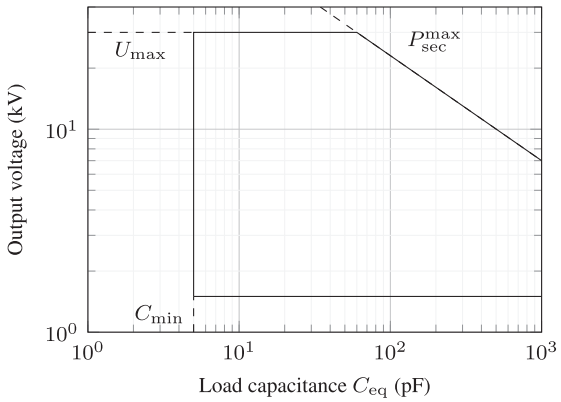

FIGURE 4 | Load diagram of the designed transformer system (see parameters in Section 5). Operation outside the indicated operating area may be possible with waveform distortion or partial discharges.

- Quality factor (i.e., losses) of the transformer,
- Thermal performance,
- Insulation system and secondary winding design.

The limiting curves of the load diagram should be designed to allow for testing at the desired voltage U_{max} with a maximum load capacitance C_{max} and test frequency f_{max}. The minimum load capacitance C_{min} is equal to the self-capacitance of the system. The secondary power limit P^{max}_{sec} will be discussed in a subsequent section.

The following sections describe the design of a ferrite-based resonant transformer, aiming to generate an HF voltage of at least 20 kV_{pk}.

3.1 | Parameter Calculation

The required leakage inductance of the resonant transformer follows directly from the range of the test frequency and the available load capacitance consisting of the DUT capacitance C_{DUT} and the optional variable capacitor C_{res} using Equation (9).

$$L_{eq} = \frac{1}{(2\pi f)^2 C_{eq}}. \tag{9}$$

The secondary current increases with frequency and capacitive load and is given by Equation (10) when the resistive component of the DUT is neglected.

$$I_s = 2\pi f C_{eq} U_o. \tag{10}$$

Where I_s is the secondary current and U_o is the output voltage.

3.2 | Core Selection

A split winding configuration creates a large leakage inductance with the windings on two legs of a UU-shape core. The desired leakage inductance can be realised with a large number of secondary turns. In addition, a large window area is needed to ensure sufficient clearance between the secondary winding and core. The split configuration aids in increasing the clearance between the primary and secondary windings.

Core saturation is not a major concern because the voltage applied to the primary is low (gain is on the order of 10^3), and the number of turns is relatively high. The flux density B in the core is calculated using the primary volt-seconds in Equation (11), where U_p is the primary peak voltage, N_p is the primary turns, and A_e is the effective core area.

$$B = \frac{U_p}{\sqrt{2}\pi f N_p A_e}. \tag{11}$$

3.3 | Leakage Inductance Estimation

No analytical formulas are currently available for the split winding configuration chosen for the resonant transformer. Attempts have been made, but are generally inaccurate [13, 14]. Therefore, the leakage inductance is simulated using a finite element model (FEM), as shown in Figure 5.

The model uses a single homogenised volume to model the secondary winding. This approach has been verified against more detailed models for a low number of turns (multiple layers and each winding modelled as a realistic wire). The simplified model has an error of below 6% in a fraction of the computation time, which is satisfactory for the leakage inductance estimate. The results are compared and shown in Figure 5 and Table 1.

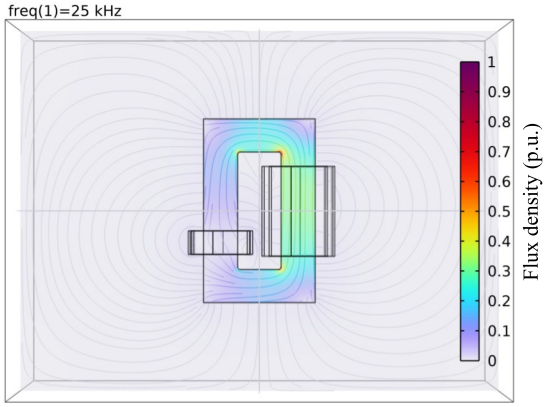

FIGURE 5 | FEM model for leakage inductance with excitation current in the secondary winding and short-circuited primary winding (50:600). The contour and colour map show the H and B-field, respectively. The colour is given in p.u. since its magnitude depends on the excitation.

3.4 | AC Resistance Estimation

Because many turns can be required to obtain the desired resonance frequency and leakage inductance, multi-layer windings are usually necessary. If the designs are limited to a single layer, very thin windings must be created, negatively impacting the corona inception voltage and winding resistance. Since the desired operating frequencies are in the range of 25–50 kHz, the skin and proximity effect should be taken into account to determine the gain of the system correctly. The AC resistance R_{AC} can be estimated using the procedure presented by Biela [15].

$$R_{AC}(f) = 2R_{DC}\left[F_R(f) + N^2 G_R(f)\frac{4M^2 - 1}{12 b_F^2}\right], \tag{12}$$

where $F_R(f)$ and $G_R(f)$ represent the skin and proximity effect, N is the number of turns per layer, M is the number of layers and b_F is the winding height. The DC resistance R_{DC} is calculated from the winding geometry and wire diameter d_{Cu}. The results shown in Figure 6 show good agreement between the measured and calculated AC resistance. For multi-layer windings, the resistance increases significantly with frequency owing to the proximity effect. Using a small wire in a single-layer winding results in less variation with frequency but limits the number of turns.

3.5 | Resonant System Gain

The gain of the resonant system depends on the turns ratio n of the transformer, as well as the quality factor Q of the system

TABLE 1 | Comparison of detailed and simplified FEM simulation results.

	Value		
Parameter	**Case 1**	**Case 2**	**Case 3**
Turns ratio N_p:N_s	10:10	10:20	10:30
Detailed winding (μH)	3.9	11.3	19.9
Simplified winding (μH)	4.1	11.5	20.1
Error (%)	+5.1	+1.8	+1.0

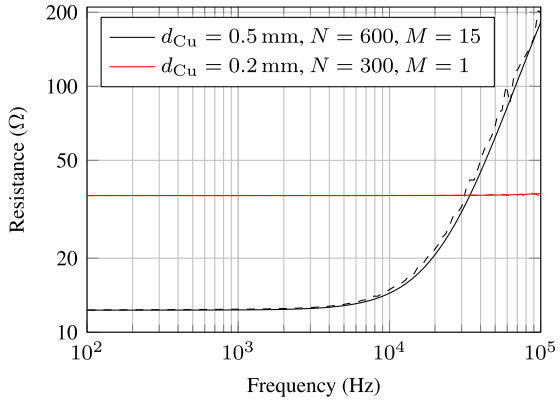

FIGURE 6 | AC resistance calculation (solid line) and measurement (dashed line) on two secondary winding designs.

(e.g., the resonant gain). The latter is determined by the combination of the transformer Q_T and the load Q_{load} (DUT and resonant capacitor), as calculated in Equation (13) derived from Equation (8).

$$Q = Q_T || Q_{load} = \left(\frac{1}{Q_T} + \frac{1}{Q_{load}} \right)^{-1}. \tag{13}$$

The gain can then be expressed as $G = nQ$. With a well-designed transformer (i.e., with high Q_T), the DUT usually determines the value of Q.

3.6 | Transformer Turns Ratio

The secondary number of turns is selected based on the FEM simulation as discussed in Section 3.3. With the preceding calculation results, the turns ratio and number of primary turns can be chosen. To achieve the desired output voltage from a source with limited output voltage, a minimum n is required. On the other hand, the secondary current is reflected back to the primary, leading to a maximum n for a current-limited source.

$$n \geq \frac{1}{Q} \frac{U_o^{max}}{U_i^{max}}, \tag{14}$$

$$n \leq \frac{I_{src}^{max}}{I_s^{max}}, \tag{15}$$

where U_i is the input voltage, and I_{src} is the current from the DC source. The superscript 'max' indicates the maximum value.

3.7 | Core Grounding

If the potential of the core is not defined, it will be determined by the parasitic capacitances between the windings and the core. This may cause the core to attain a high potential [16]. For testing at voltages below 10 kV_{pk}, this is not typically a problem. However, to avoid partial discharge (PD) between the core and LV winding, the core should be grounded [17].

If the core halves of the transformer are grounded by the copper foils, as shown in Figure 7, the gain of the resonant transformer is reduced significantly. This phenomenon can be explained as follows: Due to the large secondary leakage magnetic field, eddy currents are induced in the foils. The losses generated by these eddy currents can significantly reduce the quality factor of the transformer.

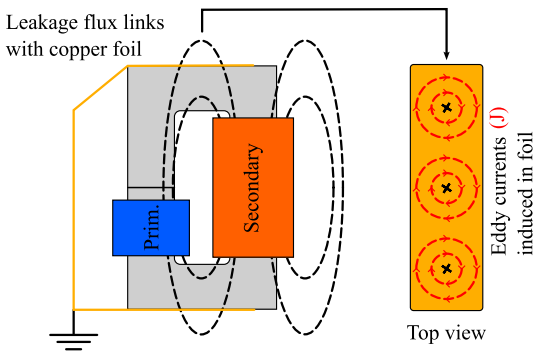

FIGURE 7 | Schematic of transformer grounding using a copper foil.

Two methods are implemented in Figure 8 to reduce the eddy current losses: First, the cross-sectional area in which the eddy current can circulate is reduced by using narrow copper wires instead of a wide foil. Second, these wires are placed far from the secondary winding to reduce the linking leakage flux.

4 | Secondary Insulation Design

Special attention must be paid to the secondary winding design. Due to the relatively small window area of the core halves, the desired HV output voltage may have the possibility to flash over across the winding or to the core.

4.1 | Bobbin Design

A disc-type structure is chosen for the secondary winding, with the number of discs selected to limit the maximum turn-to-turn voltage. A single isolation turn between adjacent discs separates the wire bundles and eliminates disc-to-disc discharges. Figure 9

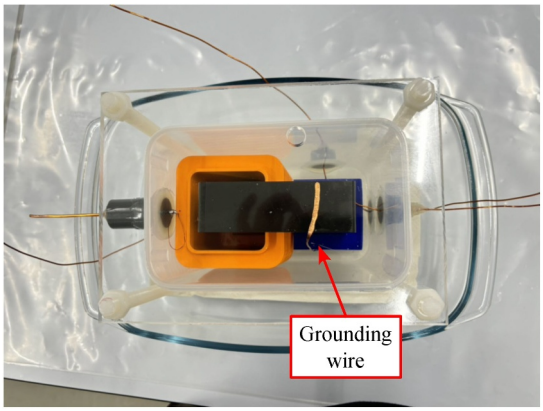

FIGURE 8 | Resonant transformer grounded by thin wires to the top and bottom core half.

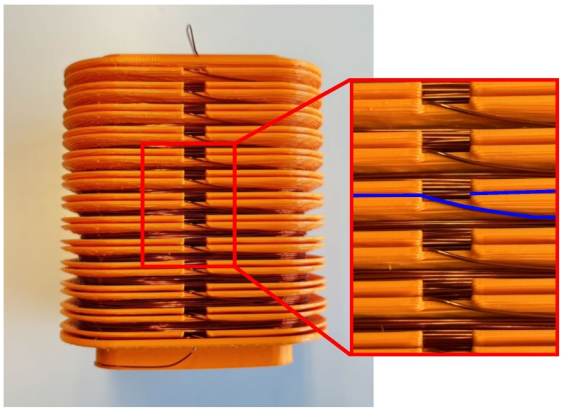

FIGURE 9 | Resonant transformer secondary winding with isolation turns in the inter-segment slots. One of the isolation turns is highlighted in blue.

shows the designed secondary bobbin with rounded corners and sufficient disc-to-disc distance to prevent flashovers.

The wire used to construct the secondary winding has a breakdown voltage of 3.3 kV_{pk}. Since the turns are wound manually in a semi-random pattern, the chance of the disc voltage occurring between neighbouring turns is small. Nevertheless, to minimise discharges between the turns, the secondary winding is divided into 12 segments to limit the disc voltage to 1.7 kV_{pk} at an output voltage of 20 kV_{pk}. Although this is around 50 % of the breakdown voltage of the wire, this potential difference will never occur in practice.

4.2 | Insulation Design

When using the designed bobbin in air, discharges may occur in the winding and between the winding and the grounded core at relatively low voltages due to the sharp edges of the core. An additional insulating material prevents these discharges while providing adequate heat dissipation from the secondary winding. For the desired output of 20 kV_{pk}, the required secondary power is already 10 kVA at $C_{eq} = 180$ pF and $f = 45$ kHz. Some inspiration for the insulation design is taken from high-power solid-state transformers. In the power range of 15–60 kVA, several different types of insulating materials are used: silicone gel [18], oil-impregnated paper [19], silicone rubber [20] and epoxy resin [20, 21]. The insulator should provide good cooling (conduction for solids or convection for liquids).

Therefore, two types of dielectrics are considered for the design of the HF resonant transformer: liquid (transformer oil and silicone oil) and solid (epoxy CY225 and silicone rubber). Liquid dielectrics offer good breakdown strength, recovery after breakdown and provide excellent cooling by convection of the insulated equipment [9]. According to the measurement results in Table 2, they have a very low dissipation factor tan δ at high frequency. The dielectric constants ε_r are similar. Solid insulation offers several benefits over liquid dielectrics: they allow for compact insulation systems, are easy to work with and maintain and are environmentally friendly. The dielectric properties of solid dielectrics are typically better and more stable over temperature. Solid insulation can only provide cooling by conduction and is typically modified with fillers to increase the thermal conductivity κ. In addition, they can be more resistant to environmental factors such as moisture and contaminants [22].

TABLE 2 | Insulation material properties (refer to Figure 16).

Material	ε_r	tan δ (10^{-4}) @ 10 kHz	κ (W/(mK))
Transformer oil	3.2	1.6	0.14
Silicone oil	2.7	3.0	0.15
Epoxy CY225+HY925	2.8	100	0.21
Silicone rubber	3.1	25	0.30

Transformer oil is chosen as the insulating liquid for the prototype transformer because of the good insulation properties, low dielectric losses and good cooling performance.

5 | Experimental Results

5.1 | Prototype Transformer

A prototype transformer was designed for the parameters presented in Table 3. Parameters with an asterisk are design targets. The maximum required test power is around 10 kVA and the secondary output current is 0.71 A_{rms}.

The transformer uses two U93/76/30 core halves of material 3C90 (permeability ≈1900) owing to the sufficient window area. A 26 AWG MW35-C wire was chosen for the HV winding, resulting in a current density of 5.1 A/mm^2. According to the FEM simulation result, the number of secondary turns should be 600 to reach the desired leakage inductance of approx. 130–140 mH, which is computed based on the frequency and load capacitance C_{eq} range. Based on the primary source limitations, a turns ratio of 12 was chosen, resulting in 50 primary turns. The bobbin is 3D printed according to the design presented in Section 4. Transformer oil of type MIDEL 7131 is used as the insulating liquid. The prototype transformer is depicted in Figure 10.

TABLE 3 | Prototype system parameters.

Parameter	Description	Value
U_o^* (kV_{pk})	Output voltage	20
f^* (kHz)	Frequency	30–45
C_{load} (pF)	Load capacitance	100–180
Q_{load}	Load quality factor	≥ 55
U_i (V_{pk})	Input voltage	≤ 30
I_{src} (A)	Input current	≤ 9

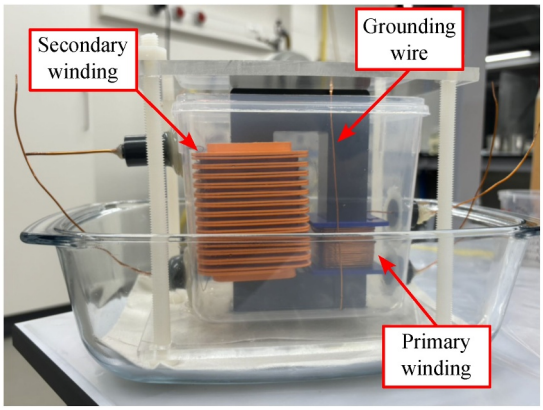

FIGURE 10 | Transformer prototype with a plastic tank for transformer oil.

5.2 | Transformer Parameter Extraction

The equivalent circuit parameters of the designed resonant transformers are extracted using the procedure of ref. [1] and presented in Table 4. The winding resistances are measured at 25 kHz. The secondary leakage inductance L_{21} obtained from the FEM simulation described in Section 3 is 139.2 mH, which is an error of less than 5% compared to the measurement. Both results lie within the range of the required L_{eq}. Using the extracted parameters and characteristics of the driving circuit, the load diagram of Figure 4 is derived.

Although the physical construction is small, the parasitic capacitance C_σ is extremely small compared to the capacitance of a reasonable DUT, which is typically more than 50 pF. Provided that the transformer is constructed properly, this dispels reason (ii) given in Section 1.1.

5.3 | Resonant Transformer Response

Next, the response of the resonant transformer is measured by exciting the primary with a small square wave voltage and measuring the peak output voltage of the transformer. The gain is calculated from the output voltage and the fundamental component of the input voltage. The measured resonance peak is compared to the analytical results of Equations (5) and (8) and shown in Figure 11. When dielectric loss is accounted for, the measured result matches the response predicted by Equation (8). The measured gain corresponds well to the calculated $G = nQ \approx 12 \times 57 = 680$, where Q is predominantly determined by Q_{load}.

TABLE 4 | Extracted transformer parameters.

Parameter	Measured value	Calculated value	Error
L_{m}	3.3 mH	3.5 mH	+6.0 %
L_{21}	133.8 mH	139.2 mH	+4.0 %
R_{11}	0.11 Ω	0.12 Ω	+9.1 %
R_{21}	27.3 Ω	25.3 Ω	−7.3 %
C_σ	5.8 pF		

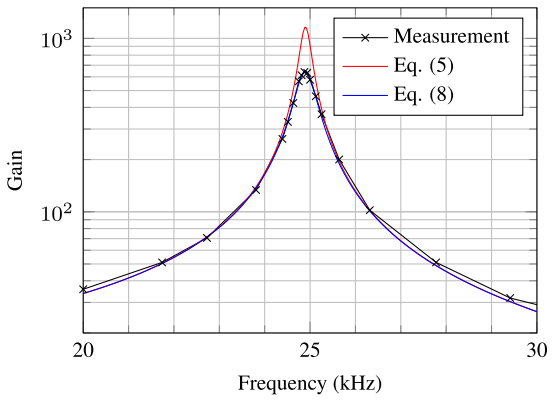

FIGURE 11 | Response of the transformer with a load consisting of the DUT ($C_{\text{DUT}} = 170$ pF, $\tan\delta = 300 \cdot 10^{-4}$ @ 25 kHz) and an additional $C_{\text{res}} = 120$ pF with no dielectric loss.

The harmonic content of the output waveform has an important effect on the insulation lifetime. Ideally, a pure sinusoidal voltage should be obtained from the resonant transformer. In Figure 12, the harmonic content is shown in the case of (i) sinusoidal primary voltage and (ii) square-wave primary voltage. As expected, the harmonics produced by the resonant test system are negligible.

The output voltage of the resonant transformer is approximately linear with the input voltage, as shown in the input–output characteristic in Figure 13. The gain of the linear fit is $G \approx 790$ V/V. Experiments on various materials have shown that the gain and linearity are heavily dependent on the properties of the DUT.

5.4 | Breakdown Characteristics of Insulated Twisted Wires

In transformer and electrical machine applications, enamelled copper wires are wound on a coil former or magnetic core. In this configuration, there will be contact points between neighbouring turns with a potential difference between them. To evaluate the breakdown behaviour of such a configuration at high frequencies, the twisted-wire samples shown in Figure 14

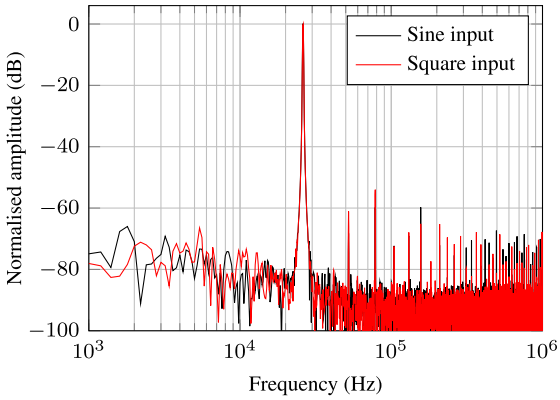

FIGURE 12 | Frequency spectrum of the output voltage of the resonant transformer driven by a square-wave (red, THD = 0.3 %) and sinusoidal voltage (black, THD = 0.2 %).

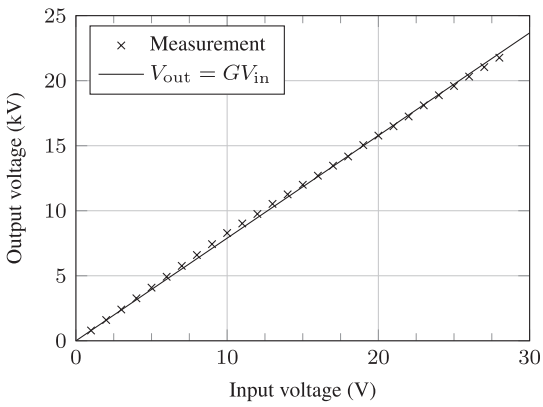

FIGURE 13 | Input–output characteristic of the resonant transformer system when driven with an inverter with variable DC link voltage.

are made of 26 AWG enamelled copper wire (MW35-C heavy film). To homogeneously distribute the contact points, strands are finely twisted. To prevent the discharges between the non-insulated ends of the wire, these are physically separated.

Twisted wire samples are submerged in oil or cast in one of the solid dielectrics. The samples are then subjected to a 35-kHz sinusoidal voltage waveform with linearly increasing amplitude. The sample breakdown voltages are analysed using Weibull statistics in Figure 15.

The breakdown results show two interesting conclusions: First of all, transformer oil has the highest breakdown voltage, even though it is one of the most lossy materials under consideration. Second, silicone rubber performs better than epoxy, which agrees with the general idea that lower-loss material should perform better under HF electrical stress. In the next paragraph, these statements are confirmed through dielectric spectroscopy. Besides a low dielectric loss, high thermal conductivity is also desired for insulation materials used at high frequencies.

5.4.1 | Relation to Material Properties

The dielectric spectrum of cylindrical raw material samples was recorded using the Novocontrol dielectric spectrometer, shown in Figure 16. The linear behaviour of the permittivity of transformer oil and silicon oil versus frequency is due to their simple molecular structures and minimal dipolar relaxation mechanisms, resulting in stable dielectric properties over a wide frequency range. In contrast, epoxy resin and silicon rubber exhibit nonlinear permittivity and loss behaviour after 1 kHz due to their complex molecular structures, leading to frequency-dependent dielectric relaxation processes that become prominent at higher frequencies.

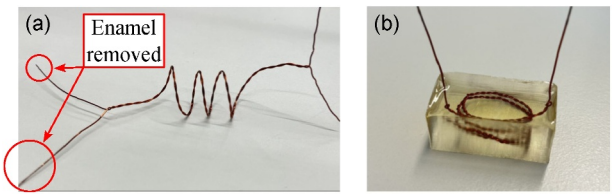

FIGURE 14 | Twisted-wire samples used for breakdown tests in (a) liquid dielectric and (b) epoxy/silicon rubber.

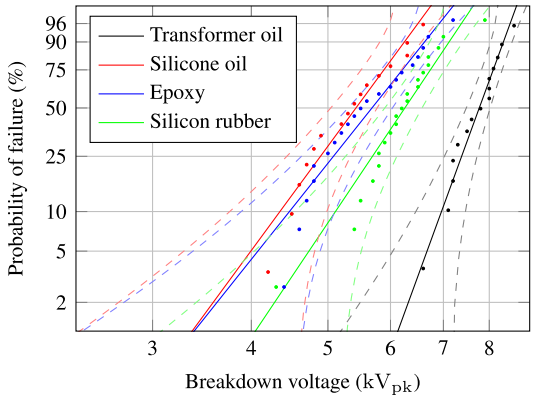

FIGURE 15 | Weibull analysis of the breakdown voltage of the twisted wires. The dashed lines mean the confidence interval.

Both dielectric liquids have a low tan δ in the range of interest (10–100 kHz). The big difference in viscosity causes the significant difference in breakdown voltage between transformer and silicone oil: transformer oil is much less viscous and, therefore, provides better convective cooling. In the range of interest, the dielectric loss tan δ of epoxy (1.0%) is significantly higher than that of silicone rubber (0.2%). Since the two materials have similar thermal conductivity, silicone rubber is less prone to thermal runaway breakdown.

The permittivity ε_r of the materials is similar, meaning that there will not be a significant difference in the parasitic capacitance of the transformer. This property has a minor influence on the resonance frequency.

6 | Discussion

A resonant test system is designed to generate a high-voltage, high-frequency sinusoidal waveform for insulation testing. The system topology, transformer secondary winding design and insulation material selection are crucial to achieving an efficient and steady test system operation.

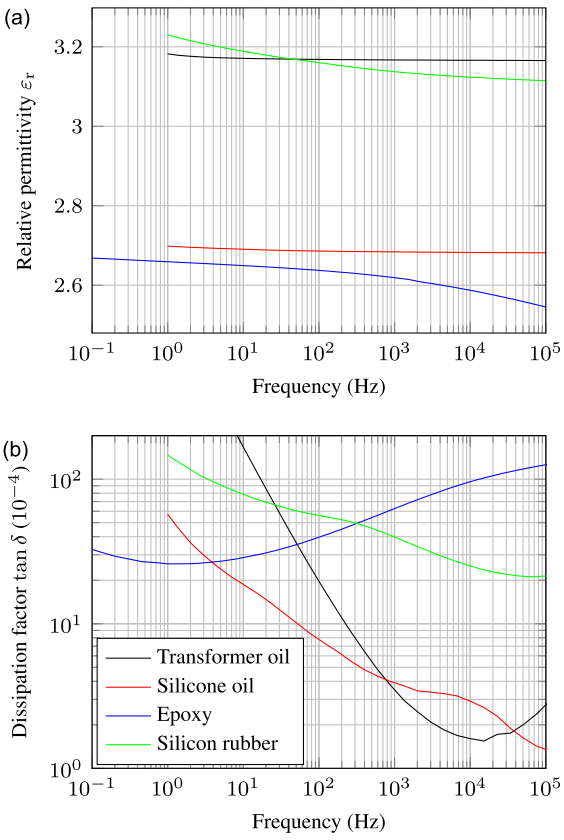

FIGURE 16 | Dielectric spectrum of evaluated insulation materials. (a) Dielectric constant ε_r and (b) dissipation factor tan δ. Parts (a) and (b) share the same legend.

6.1 | Transformer Secondary Winding Optimisation

The secondary voltage distributes nonuniformly along the disc winding, and the winding discs adjacent to the HV input take most of the voltage drop, meaning discharges and breakdown are more likely to occur [23]. Thus, an extra isolation turn is introduced; see Figure 9. This isolation turn is wrapped around the bobbin once to ensure that the last turn of the upper disc segment does not touch the adjacent lower disc segment. Without this single isolation turn, the disc-to-disc discharges will likely occur between adjacent discs at the HV side. Sufficient distance is also provided to reduce the probability of flashover.

6.2 | Loss Considerations

The losses generated in the resonant test system decrease the system output gain G and could lead to the thermal breakdown of the system components. The losses are categorised into dielectric losses (e.g., the DUT and transformer insulation) and losses in system components (e.g., amplifier and resonant capacitor). Measurement results shown in Figure 11 indicate that the DUT can be lossy. Additionally, analytical results illustrated in Figure 6 confirm that the AC resistance of the secondary winding will be large at high frequency due to the skin and proximity effect, which results in a large amount of secondary winding losses. An insulation material with low tan δ is chosen for the resonant transformer to reduce the losses. Based on Figure 16b, the transformer oil of type MIDEL 7131 is selected due to its low tan δ in the 10–100 kHz range.

Of the two resonant test systems presented in Figure 1, the inverter-based system requires much less driving current than that based on a linear power amplifier, as shown in Figure 17. Therefore, the inverter-based system is preferred. As shown in Figure 13, a stable system output gain G can be achieved with the inverter-based test system.

6.3 | System Topology Considerations

The frequency of the proposed test system is tuned using a variable capacitance. The mechanical construction of such a system is more straightforward than an inductance-tuned system, which is more common for 50/60 Hz testing. The fringing losses associated with the variable air gap are eliminated. The secondary leakage of the transformer is used as the resonant inductance. As shown in Figure 12, the quality of the output waveform is excellent, with negligible system-induced harmonics.

In the current implementation, the stability of the output amplitude and system resonant frequency is not yet guaranteed. Dielectric losses and temperature fluctuations in the DUT and variable capacitor can influence these parameters. Therefore, a closed-loop control system should be implemented to ensure a stable output voltage over time.

Due to the losses in the transformer, changing the leakage inductance is better than increasing the capacitive tuning range to achieve a larger test frequency range. This variable leakage inductance can be realised using separate transformers or by switching segments of the secondary winding (i.e., tuning the number of secondary turns).

6.4 | Resonant Test System Output Limitations

The maximum output voltage of the system depends on many factors related to the transformer and the load, as described in the load diagram in Figure 4. The auxiliary components, such as insulators, tuning capacitors and HV probes, can also have a considerable impact. All auxiliary components must be PD-free at the desired frequency and voltage. In Figure 18, HV waveforms captured using two different probes (Elditest GE3830 and North Star VD-100) are shown. Some distortion is present on the GE3830 waveform, which is attributed to PD. The voltage amplitude on the negative half-cycle is reduced from the zero crossing until the peak, indicating that PDs take energy from the resonant circuit during this period. With a suitable, PD-free high-voltage probe, operation up to 23 kV_{pk} was achieved at approximately 35 kHz (red waveform). The waveform is perfectly sinusoidal without any distortion. Higher voltages could be achieved if a DC supply with a larger output voltage capability is used.

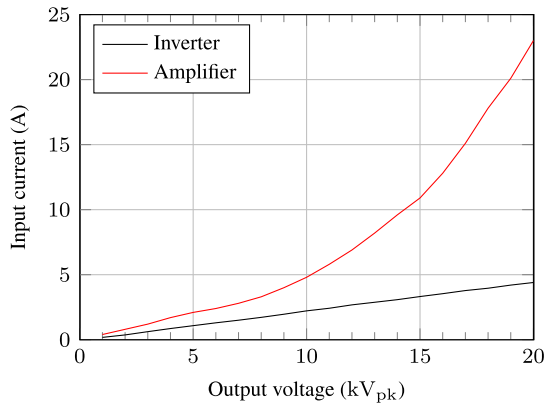

FIGURE 17 | Low-voltage current draw versus output voltage for the inverter and linear amplifier-based test systems.

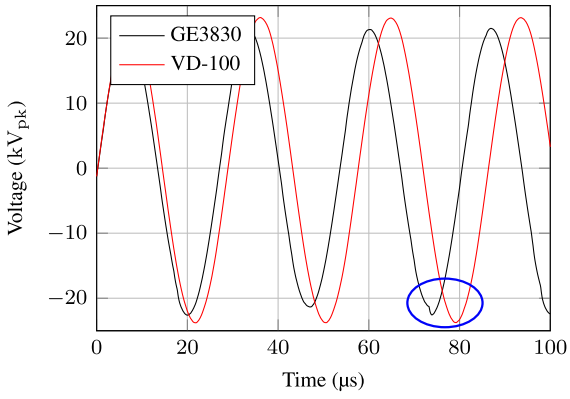

FIGURE 18 | Output voltage waveforms measured with two high-voltage probes: Elditest GE3830 and North Star VD-100. Note the PD distortion at the peaks of the waveform captured using GE3830.

7 | Conclusion

A capacitance-tuned resonant test system based on a ferrite transformer has been designed and validated. This test system can generate an HV-HF sinusoidal output waveform with an amplitude up to 23 kV_{pk} in the frequency range of 30–45 kHz. The waveform has very low distortion. The system can be driven with a power electronic inverter or a linear power amplifier, although the latter has a comparable larger current draw. The resonant transformer within the system is insulated by the transformer oil of type MIDEL 7131, which has excellent dielectric characteristics. Also, its secondary winding has been optimised using an extra isolation turn to separate the adjacent disc segments and avoid the occurrence of disc-to-disc discharges. PD-free auxiliary components are required to obtain a stable, undistorted, high-voltage output.

Acknowledgements

The authors express their appreciation for the material and financial support of the High Voltage Technology group of the Delft University of Technology and Prodrive Technologies.

Conflicts of Interest

The authors declare no conflicts of interest.

Data Availability Statement

The data that support the findings of this study are available from the corresponding author upon reasonable request.

References

1. G. W. Lagerweij, *Reliability and Ageing of IMS PCBs in High-Voltage Power Electronic Applications* (Delft University of Technology, 2023).

2. W. Zhao, T. Luo, and M. G. Niasar, "Ramp Sinusoidal Breakdown of Epoxy Resin Under High Voltage Waveforms at Different Frequencies," in *22nd International Symposium on High Voltage Engineering (ISH 2021)*, (2021), 2083–2088.

3. F. A. Dragonas, G. Neretti, P. Sanjeevikumar, and G. Grandi, "High-Voltage High-Frequency Arbitrary Waveform Multilevel Generator for DBD Plasma Actuators," *IEEE Transactions on Industry Applications* 51, no. 4 (2015): 3334–3342.

4. S. A. Saleh, B. Allen, E. Ozkop, and B. G. Colpitts, "Multistage and Multilevel Power Electronic Converter-Based Power Supply for Plasma DBD Devices," *IEEE Transactions on Industrial Electronics* 65, no. 7 (2018): 5466–5475.

5. D. A. Ganeshpure, T. B. Soeiro, M. Gagic, M. G. Niasar, P. Bauer, and P. Vaessen, "Modular Multilevel Converter-Based Arbitrary Wave Shape Generator Used for High Voltage Testing," in *2021 IEEE 19th International Power Electronics and Motion Control Conference (PEMC)*, (2021), 124–131.

6. K. Elanseralathan, M. J. Thomas, and G. R. Nagabhushana, "Breakdown of Solid Insulating Materials Under High Frequency High Voltage Stress," in *Proceedings of the 6th International Conference on Properties and Applications of Dielectric Materials (Cat. No.00CH36347)*, Vol. 2 (IEEE, 2000), 999–1001.

7. IEC TC 109, "Insulation Coordination for Equipment Within Low-Voltage Systems – Part 4: Consideration of High-Frequency Voltage Stress," *International Electrotechnical Commission* (2005): 60664–4.

8. A. Patil, *Development of Resonance-Based Test System to Measure Lifetime Curves of Dielectric Materials* (Delft University of Technology, (2022).

9. F. H. Kreuger, *Industrial High Voltage: 4. Coordinating, 5. Testing, 6. Measuring* (Delft University Press, 1992).

10. W. Hauschild and E. Lemke, *High-Voltage Test and Measuring Techniques*. 2nd ed. (Springer, 2019).

11. W. Pfeiffer, "High-Frequency Voltage Stress of Insulation. Methods of Testing," *IEEE Transactions on Electrical Insulation* 26, no. 2 (1991): 239–246.

12. N. Hardt and D. Koenig, "Testing of Insulating Materials at High Frequencies and High Voltage Based on the Tesla Transformer Principle," in *Conference Record of the 1998 IEEE International Symposium on Electrical Insulation (Cat. No.98CH36239)*, Vol. 2 (1998), 517–520.

13. D. Azizian, M. Vakilian, J. Faiz, and M. Bigdeli, "Calculating Leakage Inductances of Split-Windings in Dry-Type Traction Transformers," *ECTI Transactions on Electrical Engineering, Electronics, and Communications* 10, no. 1 (2012): 17–24.

14. R. Schlesinger and J. Biela, "Comparison of Analytical Models of Transformer Leakage Inductance: Accuracy Versus Computational Effort," *IEEE Transactions on Power Electronics* 36, no. 1 (2021): 146–156.

15. J. Biela, "Optimierung des elektromagnetisch integrierten serien-parallel Resonanzkonverters mit eingeprägtem Ausgangsstrom [Doctoral Thesis]," *ETH Zürich* (2005): 235–240.

16. P. Mathew, M. G. Niasar, and P. Vaessen, "Design of High-Frequency Fast-Rise Pulse Modulators for Lifetime Testing of Dielectrics," *IEEE Transactions on Dielectrics and Electrical Insulation* 30, no. 6 (2023): 2798–2808.

17. Y. Kawaguchi, K. Furukawa, T. Shimada, and J. Kusukawa, "Feasibility Study of High-Frequency Transformer With High-Voltage Insulation Structure for SST Based Medium-Voltage Multi-Level Converter," in *2022 International Power Electronics Conference (IPEC-Himeji 2022-ECCE Asia)*, (2022), 1769–1774.

18. C. Zhao, Y. Hsieh, F. C. Lee, and Q. Li, "Design and Analysis of a High-Frequency CLLC Resonant Converter With Medium Voltage Insulation for Solid-State-Transformer," in *2021 IEEE Applied Power Electronics Conference and Exposition (APEC)*, (2021), 1638–1642.

19. M. Kharezy, H. R. Mirzaei, Y. Serdyuk, T. Thiringer, and M. Eslamian, "A Novel Oil-Immersed Medium Frequency Transformer for Offshore HVDC Wind Farms," *IEEE Transactions on Power Delivery* 36, no. 5 (2021): 3185–3195.

20. Z. Yi, K. Sun, Z. Dang, and Y. Song, "Design of Medium-Voltage High-Frequency Transformers Based on High-Thermal-Conductivity Insulation Material," in *2023 IEEE PELS Students and Young Professionals Symposium (SYPS)*, (2023), 1–6.

21. K. T. Chen, J. F. Chen, T. J. Wang, and H. Liao, "Study and Implementation of High Frequency Cast Resin Transformer Applied for Medium-Voltage Solid-State Transformer," in *2021 IEEE International Future Energy Electronics Conference (IFEEC)*, (2021), 1–6.

22. I. A. Tsekmes, R. Kochetov, P. H. F. Morshuis, and J. J. Smit, "A Unified Model for the Permittivity and Thermal Conductivity of Epoxy Based Composites," *Journal of Physics D Applied Physics* 47, no. 41 (2014): 415502.

23. M. Ghaffarian Niasar and W. Zhao, "Impulse Voltage Distribution on Disk Winding: Calculation of Disk Series Capacitance Using Analytical Method," in *2020 IEEE International Conference on High Voltage Engineering and Application* (ICHVE, 2020), 1–4.